Synthesis and Evaluation of *N*-Methyl and *S*-Methyl ^{11}C-Labeled 6-Methylthio-2-(4′-*N*,*N*-dimethylamino)phenylimidazo[1,2-*a*]pyridines as Radioligands for Imaging β-Amyloid Plaques in Alzheimer's Disease

Lisheng Cai,*,† Jeih-San Liow,† Sami S. Zoghbi,† Jessica Cuevas,† Cesar Baetas,† Jinsoo Hong,† H. Umesha Shetty,† Nicholas M. Seneca,† Amira K. Brown,† Robert Gladding,† Sebastian S. Temme,† Mary M. Herman,‡ Robert B. Innis,† and Victor W. Pike†

Molecular Imaging Branch and Clinical Brain Disorders Branch, National Institute of Mental Health, National Institutes of Health, Bethesda, Maryland 20892

Received August 4, 2007

6-Thiolato-substituted 2-(4′-*N*,*N*-dimethylamino)phenylimidazo[1,2-*a*]pyridines (*RS*-IMPYs; **1**−**4**) were synthesized as candidates for labeling with carbon-11 ($t_{1/2}$ = 20.4 min) and imaging of A_β plaques in living human brain using positron emission tomography (PET). K_i values for binding of these ligands to Alzheimer's disease brain homogenates were measured in vitro against tritium-labeled **6** (Pittsburgh compound B). MeS-IMPY (**3**, K_i = 7.93 nM) was labeled with carbon-11 at its *S*- or *N*-methyl position to give [^{11}C]**7** or [^{11}C]**8**, respectively. After injection into rats, [^{11}C]**7** or [^{11}C]**8** gave moderately high brain uptakes of radioactivity followed by rapid washout to low levels. The ratio of radioactivity at maximal uptake to that at 60 min reached 18.7 for [^{11}C]**7**. [^{11}C]**7** behaved similarly in mouse and monkey. [^{11}C]**7** also bound selectively to A_β plaques in post mortem human Alzheimer's disease brain. Although rapidly metabolized in rat by N-demethylation, [^{11}C]**7** was stable in rat brain homogenates. The ex vivo brain radiometabolites observed in rats have a peripheral origin. Overall, [^{11}C]**7** merits further evaluation in human subjects.

Introduction

A key event in the pathogenesis of Alzheimer's disease (AD[a]) is now believed to be the deposition of β-amyloid (A_β) plaques in brain.[1,2] A "β-amyloid cascade" hypothesis has emerged to account for various experimental facts, including genetic variations related to the production and elimination of A_β.[3,4] Four inherited genes[5,6] (APP, presenilin-1, presenilin-2, and SORL1[7]) and one firmly established susceptibility gene (Apo ϵ4)[8,9] have been identified. Also, more than a further dozen potential AD susceptibility genes have been identified with statistically significant allelic summary odds ratio.[10,11] Neuritic plaques and neurofibriliary tangles are accepted pathological hallmarks of AD disease as confirmed at autopsy.[12,13] Ante mortem identification and quantification of A_β plaques would have value for both the early diagnosis of AD and the monitoring of the clinical development of therapeutic drugs targeted to arrest or eliminate A_β plaques in living brain.[14,15] At least three radioligands for positron emission tomography (PET) and one for single photon emission computed tomography (SPECT)[16] have reached the clinical stage[14,15,17] (Figure 1).

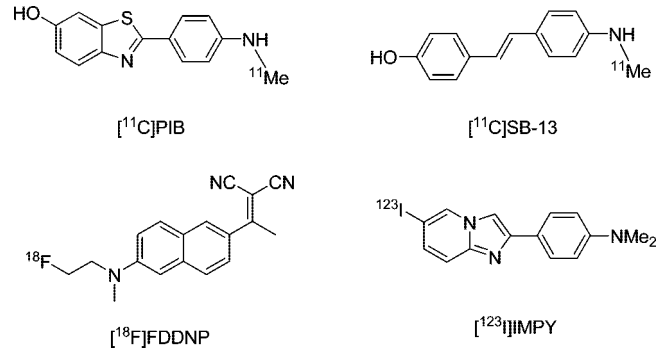

Figure 1. Three radioligands for A_β plaque imaging with PET and one for imaging with SPECT in clinical research.

Among these radioligands, [^{11}C]PIB (**6**) has been the most effective and the most thoroughly studied.[18,19] There is a clear distinction between AD subjects and normal controls in A_β-plaque load measured with this radioligand in PET imaging.[18] The ratio of radioactivity of different regions of the gray matter to that of cerebellum, the relatively plaque-free reference region, reaches about 2.5 in AD patients. Although this is a significant result in its own right, this ratio is not optimal for the two targeted purposes for A_β PET radioligands (early diagnosis and drug monitoring). The average heavy load of A_β plaques in the AD patient (about 2 μM) should permit more sensitive radioligands to be developed.[20] We aimed to develop new PET radioligands with potential to expand the dynamic range of the radioactivity ratio between cortex and cerebellum, by increasing either radioligand binding affinities or the rates of washout of radioactivity from the brain.[21] The former would increase the binding potential (BP), which is proportional to the PET signal produced, and the latter would decrease the nonspecific binding (the background noise).

* To whom correspondence should be addressed. Address: Molecular Imaging Branch, National Institute of Mental Health, National Institutes of Health, 10 Center Drive, Building 10, Room B3 C346, Bethesda, MD 20892. Phone: (301) 451-3905. Fax: (301) 480-5112. E-mail: cail@intra.nimh.nih.gov.

† Molecular Imaging Branch.

‡ Clinical Brain Disorders Branch.

[a]Abbreviations: A_β, beta amyloid; AD, Alzheimer's disease; APP, amyloid precursor protein; BP, binding potential; CA, carrier-added; $cLogD_{7.4}$, calculated logarithm of distribution coefficient between octanol and water at pH 7.4; EOS, end of synthesis; HRMS, high-resolution mass spectra; ID, injected dose; NCA, no-carrier-added; PBS, phosphate buffered saline; PET, positron emission tomography; PIB, Pittsburgh compound B; RCY, decay-corrected radiochemical yield; SAR, structure–activity relationship; SD, standard deviation; SORL1, sortolin related receptor; SPECT, single photon emission computed tomography; TAC, time−activity curve; nM, nanomolar; RT, room temperature; ppm, parts per million.

10.1021/jm700970s
Published on Web 12/14/2007

Scheme 1

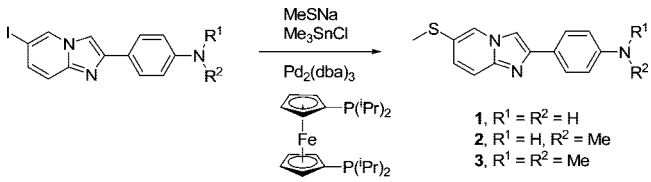

For prospective high-affinity radioligands for imaging A_β plaques with PET, the ratios of radioactivity in normal animal brains at maximal level and at a later specific time (e.g., 60 min after injection) are considered predictive of the signal-to-noise ratio that might be achievable when A_β plaques are present.[21] [^{125}I]IMPY (**5**) ([^{125}I]4-(6-iodo-*H*-imidazo[1,2-*a*]pyridin-2-yl)-*N,N*-dimethylbenzeneamine) (Figure 1) is one of the few radioligands showing a high ratio of radioactivity between 2 and 60 min[17] and is superior to [^{11}C]**6**[22] in this respect. IMPY analogues also show scope for further study of structure−affinity relationships (SAR) in order to select better ligands for A_β plaque imaging.[23,24]

We have previously evaluated two IMPY derivatives, [^{18}F]FEM-IMPY [*N*-(2-fluoroethyl)-4-(6-iodo-*H*-imidazo[1,2-*a*]pyridin-2-yl)-*N*-methylbenzeneamine] and its 3-fluoropropyl analogue, [^{18}F]FPM-IMPY, as A_β plaque PET radioligands.[25] After intravenous injection of either radioligand into rodent or monkey there is a rapid and moderately high uptake of radioactivity into the brain (∼160% SUV), followed by biphasic clearance with a fast and very slow component. Metabolism is rapid and is demonstrated in rat to involve dealkylation of the tertiary aromatic amino group, culminating in defluorination and high uptake of radioactivity ([^{18}F]fluoride ion) into bone. Tetradeuteration of the fluoroethyl group in [^{18}F]FEM-IMPY does not lead to a significant reduction in the residual brain radioactivity but reduces the bone uptake of radioactivity, presumably because of an isotope effect on metabolism. With a view to avoiding rapid defluorination and to eliminate residual radioactivity in brain, we later decided to make use of an "isoelectronic effect" in the design of further analogues of **5**.[24] We considered that this strategy might retain high binding affinity while reducing lipophilicity. Also, we have recently explored replacement of the 6-iodo group in **5** with thiolato groups, thereby opening up new possibilities for labeling with positron emitters [carbon-11 ($t_{1/2}$ = 20.4 min) and fluorine-18 ($t_{1/2}$ = 109.7 min)].[24] Here, we report the syntheses, ^{11}C-labeling, and in vitro and in vivo evaluation of new 6-thiolato-IMPY derivatives in our continuing effort to develop useful radioligands for the detection of A_β plaques in AD patients with PET.

Results

Chemistry. We used a combination of sodium methanethiolate and trimethyltin chloride to synthesize the IMPY derivatives **1**−**3** from their corresponding iodo compounds (Scheme 1). To facilitate the radiolabeling of the *S*-methyl group in **3**, we designed compound **4** (Scheme 2), a masked arylthiol compound, as the precursor for reaction with [^{11}C]iodomethane. This precursor was synthesized in high yield from **5** according to a reported general method.[26]

Binding Affinities for Human AD A_β Plaques and Lipophilicities of Ligands. The K_d value of **6** in our in vitro assay for binding to human A_β plaques was 7.23 nM. Ligand **3** exhibited an affinity comparable to that of **6** or **5** (Table 1). Ligands **1**, **2**, and **4** exhibited much lower affinity. Computed ($cLogD_{7.4}$) and measured lipohilicities ($LogD_{7.4}$) were in fair agreement for each of the ligands **1**−**4** (Table 1).

Scheme 2

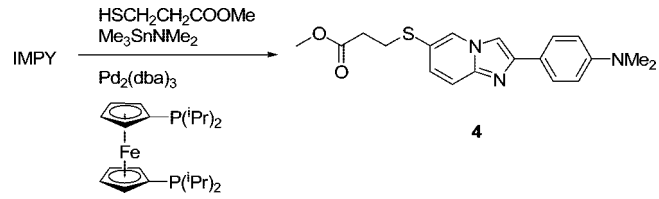

Pharmacological Screen. Ligand **3** was selective for β-amyloid plaques, since 10 μM compound caused <50% inhibition of radioligand binding to all of the large number of tested central nervous system receptors (NIMH Pharmacology Drug Screening Program). These receptors included 5-$HT_{1A,B,D,E,2A-C,3,5A,6,7}$, $\alpha_{1a,b,2a}$, β_2, D_{1-5}, H_1, and MOR.

Radiochemistry. Treatment of **4** with [^{11}C]iodomethane under basic conditions (Scheme 3) gave chemically (>95%) and radiochemically pure (>99%) [^{11}C]**7** in 10−13% decay-corrected radiochemical yield (RCY) after formulation for intravenous administration with a high specific radioactivity (1.4−2.0 Ci/μmol) at the end of synthesis (EOS). The "loop" technique reported by Wilson et al.[27] for the preparation of [^{11}C]**6** when applied to **2** gave [^{11}C]**8** in moderate RCY (5.1−17.4%) and in high chemical purity (>90%) and radiochemical purity (>99%) and with a specific radioactivity of 2.3−11.9 Ci/μmol at EOS (Scheme 4).

Stability of [^{11}C]7 in the Formulated Dose. The radiochemical purity of [^{11}C]**7** ranged between 99.2% and 94.7% immediately after radiosynthesis. This formulated radioligand (pH ∼ 7.5) was radiochemically stable for 3 h. However, when the pH of the solution was reduced immediately after preparation to ∼4.5, the radioligand decomposed to 51.2% radiochemical purity within 2 h. Immediate neutralization was therefore required after the HPLC purification of [^{11}C]**7** under acidic conditions.

Autoradiography of Human A_β Plaques with NCA [^{11}C]7 in Vitro. In vitro autoradiography of a confirmed AD brain specimen exposed to no-carrier-added (NCA) [^{11}C]**7** showed specific binding only to cortical areas containing neuritic plaques (Figure 2A); the areas of specific binding of [^{11}C]**7** matched those stained with thioflavin-S in the same tissue slides (data not shown). Specific binding of [^{11}C]**7** to regions of cortical gray matter having neuritic plaques was eliminated in an AD brain specimen pretreated with nonradioactive **3** (Figure 2B). No specific binding of NCA or carrier-added (CA) [^{11}C]**7** was observed in a control human brain specimen (Figure 2C, D).

Stability of NCA [^{11}C]7 in Rat Whole Blood, Rat Brain, and Monkey Whole Blood in Vitro. NCA [^{11}C]**7** was 91% unchanged after 60 min of incubation in rat whole blood and 93.6% unchanged after 60 min of incubation with rat brain homogenate. The radioligand was 96.2% and 94.5% unchanged after 30 and 90 min of incubation in monkey whole blood, respectively.

Evaluation of NCA [^{11}C]7 in Normal Rodents in Vivo with PET. After intravenous injection of a bolus of NCA [^{11}C]**7** into rat, there was a rapid and high uptake of radioactivity into brain followed by a rapid and continuous washout (Figure 3A). Similar time−activity curves (TACs) were observed for mice (Figure 3B). Radioactivity levels were uniform across rat and mouse brain. The ratios of brain radioactivity at maximal uptake to that at 60 min after injection of [^{11}C]**7** were 18.7 for rat and 11.1 for mouse.

Evaluation of NCA [^{11}C]8 in Normal Rat in Vivo with PET. After intravenous injection of a bolus of NCA [^{11}C]**8** into rat (Figure 4), there was rapid and high uptake of radioactivity

Table 1. K_i and measured $LogD_{7.4}$ Values of IMPY Derivatives

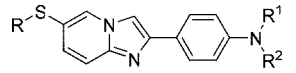

1, R = Me, R^1 = R^2 = H
2, R = Me, R^1 = H, R^2 = Me
3, R = Me, R^1 = R^2 = Me
4, R = $MeO_2CCH_2CH_2$, R^1 = R^2 = Me

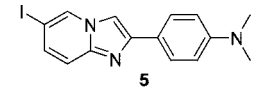

5

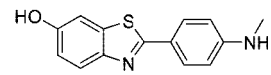

6

ligand	R	R^1	R^2	$LogD_{7.4}$[a]	$cLogD_{7.4}$[b]	K_i (nM)[c]
1	Me	H	H	2.6 ± 0.1	2.43 ± 1.3	377 ± 225
2	Me	H	Me	3.6 ± 0.1	3.24 ± 1.3	80 ± 16
3	Me	Me	Me	4.1 ± 0.1	3.67 ± 1.3	7.93 ± 0.60
4	$MeO_2CCH_2CH_2$	Me	Me	3.6 ± 0.1	3.33 ± 1.4	205 ± 56
5, IMPY				3.58 ± 0.44[25]	4.37 ± 0.88	8.95 ± 0.72
6, PIB				1.3[22]	3.33 ± 0.8	7.23 ± 0.26[d]

[a] Values are mean ± SD (n = 3). [b] Values are calculated with ACD/LogD, version 9.02 (Advanced Chemistry Development, Inc., Toronto, Canada). [c] Values are mean ± SD (n = 3). [d] K_d value is mean ± SD (n = 4).

Scheme 3

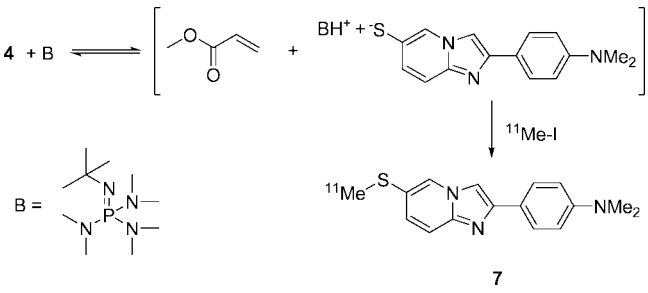

7

Scheme 4

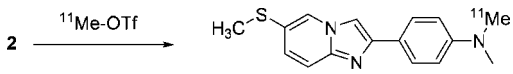

8

into the brain. This uptake was followed by washout of the majority of radioactivity over about 30 min, but thereafter the decay-corrected radioactivity remained almost constant. The ratio of radioactivity of maximal uptake to that at 60 min after injection was 6.1 for rat.

Emergence of Radiometabolites of NCA [^{11}C]7 in Normal Rat Brain, Plasma, and Urine. The radiochemical purities of the two preparations of NCA [^{11}C]**7** used in this experiment were 98% and 99%. Recoveries of rat cerebellum, forebrain, and plasma radioactivities into acetonitrile for HPLC analysis were more than 86%. Recovery of all analyte radioactivity from the HPLC was confirmed in an experiment with samples from one rat. In all the tissue and plasma samples three radiometabolites (A, B, and C) were detected, and these appeared to be less lipophilic (t_R = 2.2, 3.7, and 5.0 min, respectively) than parent radioligand (t_R = 7.6 min) in the reverse phase HPLC analysis (Figure 5). The concentrations of [^{11}C]**7** and its radiometabolites in rat tissue regions were normalized for injected dose and rat weight by conversion to % SUV (Table 2). At 2.83 min after the injection of [^{11}C]**7** into three rats, the percentages of radioactivity represented by parent radioligand in cerebellum, cerebrum, and plasma were 32.6, 30.1, and 6.5, respectively. Thirty minutes after the injection of [^{11}C]**7**, these values decreased to 18.6, 13.0, and 0.2, respectively. At this time, residual parent radioligand concentrations were very low (8.9, 5.1, and 0.2, SUV, respectively). Therefore, the effect of residual blood on the accuracy of these outcome measures was studied in one rat. Ex vivo chromatography of extracts from perfused rat cerebellum, cerebrum, and plasma showed 21.3%, 15.6%, and 0.1% of their total radioactivities to be parent [^{11}C]**7** at 30 min. These values were thus similar to those obtained in nonperfused rats. At 2.83 min the total radioactivity in urine was very low and mainly composed of radiometabolites A and B (Table 2).

Emergence of Radiometabolites of CA [^{11}C]7 in Rat Brain, Plasma, and Urine. The rat tissue concentrations of [^{11}C]**7** and of its radiometabolites at 10 min after bolus injection of CA [^{11}C]**7** (carrier dose, 22.94 μmol/kg) are shown in Table 3. The percentage of radioactivity represented by [^{11}C]**7** in cerebellar, cerebral, and plasma extracts at 10 min after injection was higher (80.9%, 83.1%, and 55.3%, respectively) in this CA experiment than in the NCA experiment. Even the urine had a higher percentage of [^{11}C]**7**.

Evaluation of NCA [^{11}C]7 in Normal Monkey with PET. TACs (time−activity curves) for brain regions of a 5 year old rhesus monkey administered intravenously with a bolus of NCA [^{11}C]**7** are shown in Figure 6A. The uptake of radioactivity into all brain regions was rapid and high. Cerebellum showed the highest uptake of radioactivity. The radioactivity washed out continuously from all brain regions and at a similar rate all over the duration of the scan. The washout was somewhat slower than in rats and mice. The ratios of radioactivity of maximal uptake to that at 60 min after injection were 9.9 for frontal cortex, 8.3 for temporal cortex, 7.6 for parietal cortex, 7.8 for occipital cortex, and 9.4 for cerebellum.

Evaluation of NCA [^{11}C]8 in Normal Monkey with PET. After intravenous injection of a bolus of NCA [^{11}C]**8** into a 9.7 kg normal monkey there was rapid and high uptake of radioactivity into the brain followed by washout to a low plateau level (Figure 7B). The ratios of the maximal radioactivity uptake to that at 60 min after injection for various brain regions were 3.5 for frontal cortex, 4.1 for temporal cortex, 3.1 for parietal cortex, 3.4 for occipital cortex, and 4.2 for cerebellum.

Emergence of Radiometabolites of NCA [^{11}C]7 in Monkey Plasma. In two monkey experiments, anticoagulated venous blood samples were drawn at 10 and 30 min after injection of NCA [^{11}C]**7** into monkey, and radio-HPLC showed at least three radiometabolites with retention times of 2.0, 3.7, and 4.9 (vs 7.4 min for [^{11}C]**7**) (Figure 7). Although [^{11}C]**7** was well-resolved from its radiometabolites, the radiometabolites were not well-resolved from each other. Between 12.4% and 17.3% (8.1% and 15.2% SUV) of the plasma radioactivity was [^{11}C]**7** at 10 min after its administration. At 30 min, 3.5–5.6% (1.8–4.2% SUV) of the plasma was [^{11}C]**7**.

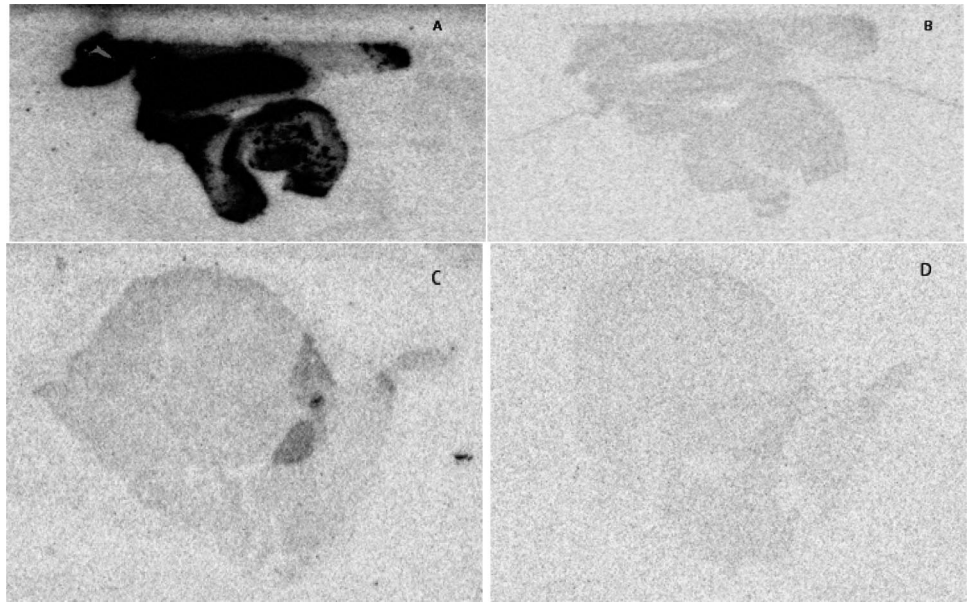

Figure 2. Autoradiographs of AD brain slices incubated with NCA [^{11}C]**7** (A) or CA [^{11}C]**7** (B) and of control human brain slices incubated with NCA [^{11}C]**7** (C) or CA [^{11}C]**7** (D).

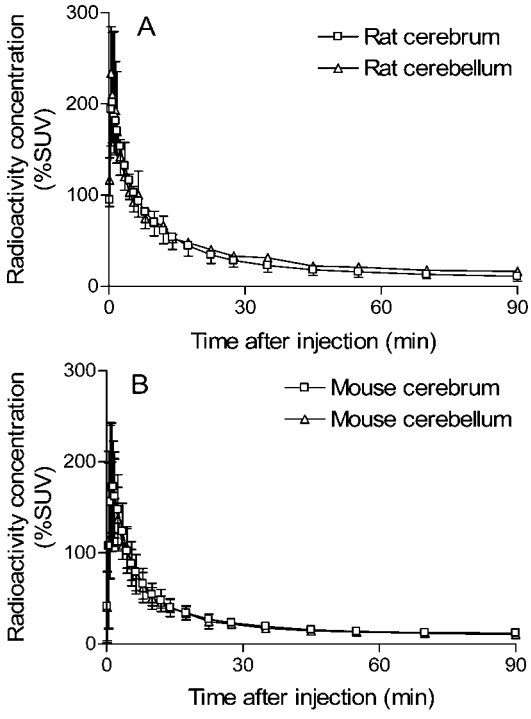

Figure 3. Time course of radioactivity (% SUV) in cerebrum and cerebellum after administration of NCA [^{11}C]**7** to normal rats ($n = 4$) (A) and normal mice ($n = 4$) (B). Unilateral error bars indicate the magnitude of SD.

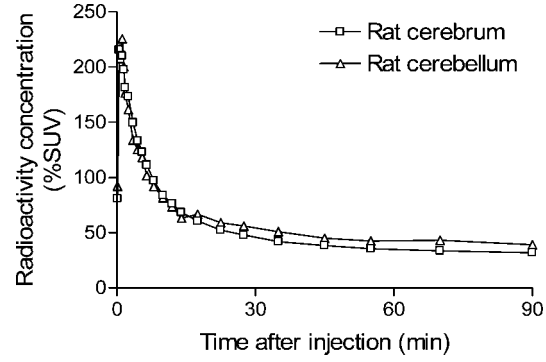

Figure 4. Time course of radioactivity (% SUV) in cerebrum and cerebellum after administration of NCA [^{11}C]**8** to normal rats ($n = 2$).

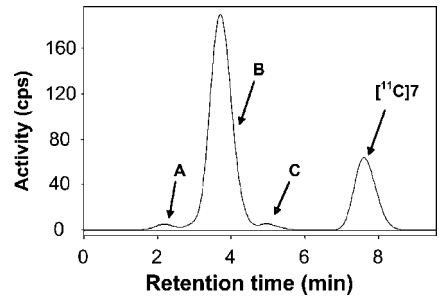

Figure 5. Radiochromatogram of a rat brain extract at 2.83 min after injection of NCA [^{11}C]**7**.

LC−MS Analysis of Rat Brain Metabolites of 3. To characterize the metabolites of **3**, CA [^{11}C]**7** was administered to a rat and HPLC fractions of brain homogenates corresponding to the radiometabolites were collected and analyzed by LC−MS. The total-ion chromatogram was searched for potential metabolite-specific ions. Fraction 1 of the brain extract (metabolite A) showed no protonated molecule, $[M + H]^+$, for any metabolite of **3** that might be generated by oxidative hydroxylation of an *N*-methyl group to produce formaldehyde, formate, or carbonate. Analysis of fraction 2 (metabolites B and C) showed a $[M + H]^+$ ion at *m*/*z* 270. This metabolite (metabolites B) eluted off the HPLC column with $t_R = 8.1$ min (mean of three analyses). MS−MS analysis of this metabolite generated product ions *m*/*z* 255, 237, and 223. In an $MS^{n(3)}$ experiment, trapping and dissociation of the most abundant ion, *m*/*z* 255, resulted in secondary product ions *m*/*z* 254, 240, 239, 228, 222, 211, 208, 151, and 131. These LC−MS data of metabolite B were in full accord with those of the reference *N*-desmethyl compound **2**.

Discussion

We have previously developed a homogeneous catalytic reaction for the substitution of an arylhalo substituent with a

Table 2. Distribution of [^{11}C]**7** and Its Radiometabolites (Mean ± SD) in Various Tissues in Rats That Were Sacrificed at Different Times after iv Injection of NCA [^{11}C]**7**

			radioactivity distribution			
time (min)	tissue	total radioactivity (%SUV)	% [^{11}C]**7**	% Met A	% Met B	% Met C
2.33	cerebrum (n = 1)	668	41.9	1.50	51.3	5.08
	plasma (n = 1)	115	9.57	23.7	60.3	6.43
2.83	cerebellum (n = 2)	261 ± 37	31.9 ± 4.9	5.85 ± 4.2	60.9 ± 0.75	1.5 ± 0.1
	cerebrum (n = 2)	392 ± 12	30.2 ± 4.5	0.550 ± 0.55	68.6 ± 3.5	0.60 ± 0.5
	plasma (n = 2)	81.3 ± 34	9.15 ± 6.5	36.6 ± 18	67.6 ± 7.5	1.6 ± 1.5
	urine (n = 1)	0.8	25.7	48.2	24.0	2.1
30	cerebellum (n = 3)	48.3 ± 0.9	18.6 ± 9.2	31.4 ± 5.7	28.3 ± 3.6	21.7 ± 7.1
	cerebrum (n = 3)	40.0 ± 7.6	13.0 ± 5.2	28.9 ± 18	24.4 ± 1.6	33.7 ± 11
	plasma (n = 3)	81.6 ± 14	0.2 ± 0.1	46.4 ± 11	34.4 ± 9.3	19.0 ± 2.1

Table 3. Distribution of CA [^{11}C]**7** and Its Radiometabolites (% SUV) in Various Rat Tissues and Fluids at 10 min after Bolus Injection[a]

		radioactivity distribution			
sample[a]	total radioactivity (% SUV)	% [^{11}C]**7**	% Met A	% Met B	% Met C
cerebellum	122	83.1	0.5	15.4	1.1
cerebrum	417	80.9	0.5	16.4	2.3
plasma	154	55.3	12.1	28.9	3.7
urine	4.7	29.7	33.5	20.2	16.7

[a] n = 1.

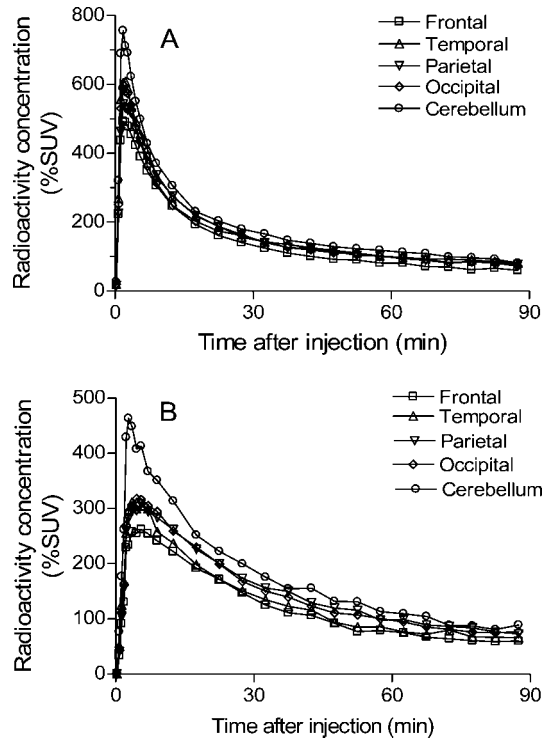

Figure 6. Time course of radioactivity (% SUV) in brain regions of a rhesus monkey after administration of NCA [^{11}C]**7** (A) or NCA [^{11}C]**8** (B).

thiolato group that avoids concomitant formation of reduced products when using thiol or thiolate as reagent.[26] Methanethiol is a gas and inconvenient for easy handling. Therefore, to synthesize *S*-methyl compounds **1**−**3**, we modified the method to use sodium methanethiolate and trimethyltin chloride as reagents instead of thiol and trimethyltin dimethylamide (Scheme 1). Low to moderate yields were achieved. The observed equivalence between thiol plus trimethyltin dimethylamide and alkali thiolate plus trimethyltin chloride as reagents expands the scope of our previously developed reaction.[26]

Since [^{11}C]**6** is the most thoroughly studied PET radioligand for the detection of A_β plaques in living human brain in vivo, we selected [^{3}H]**6** as the reference radioligand for our in vitro binding assay. A_β plaques from synthetic or transgenic rodents differ from that of AD brain in both topology and number of binding sites.[28] Therefore, we selected A_β plaques from AD brain homogenates as the closest mimic of human brain A_β plaques in vivo, for use in our assay. Binding affinity increased with the number of *N*-methyl groups in this series of IMPY derivatives (**1**−**3**) as observed for other IMPY derivatives.[23] Thus, only ligand **3** was found to have a high binding affinity similar to that of **6** and **5** (Table 1). Furthermore, the computed and measured lipophilicities of this ligand were in the range considered to be optimal for good penetration of the blood−brain barrier without excessive nonspecific binding to brain tissue (Table 1).[29,30] Therefore **3** was selected for labeling with carbon-11 and evaluation of its radioligand behavior in vitro and in vivo.

A receptor screen revealed that ligand **3** is devoid of high-affinity binding to a host of neuroreceptors and transporters in the brain. Any significant PET imaging signal compared with that of cerebellum, which is devoid of amyloid plaques in AD patients, obtained with ^{11}C-labeled **3** is therefore expected to represent binding to A_β plaques.

The successful ^{11}C-labeling of an aryl methyl thiol ether through treatment of a sulfanyl γ-propionic acid methyl ester with [^{11}C]iodomethane under basic conditions has been reported previously.[31] We sought to apply this method to the radiosynthesis of [^{11}C]**7** and for this purpose synthesized the requisite precursor **4** according to the general method that we have described for the preparation of aryl thiolates (Scheme 2).[26] The choice of base for the ^{11}C-methylation reaction was found to be critical. The synthesis of aryl thiol ethers from masked thiol esters has previously been realized with strong bases, such as KO^{t}Bu at low temperature.[32] Therefore, we initially evaluated KO^{t}Bu and a variety of other inorganic bases, such as NaOH, KOH, Cs_2CO_3, and K_2CO_3, for use in the labeling reaction. Although some labeled product was observed, the radiochemical

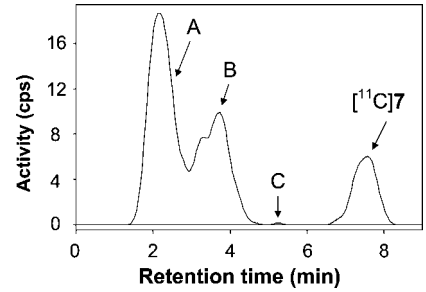

Figure 7. Radiochromatogram of a monkey plasma at 10 min after injection of NCA [^{11}C]**7**.

yields varied dramatically. Precursor also disappeared completely during these reactions. The major side reaction was ester hydrolysis to give the carboxylate salt, which was inert to any further reaction. A large strong organic base (e.g., *tert*-butylimine-tris(dimethylamino)phosphorane) was much more successful in promoting a high and consistent radiochemical yield of [^{11}C]**7**. In the absence of water, such a base avoids unwanted ester hydrolysis and favors removal of the β-proton to generate the free thiolate ion with the desired high reactivity toward [^{11}C]iodomethane. A pre-equilibrium between precursor and free thiolate ion is likely reached in the presence of such a base (Scheme 3). Formulated [^{11}C]**7** at neutral pH was stable but gradually decomposed under acidic conditions. Immediate neutralization of the acid was therefore required after the HPLC purification of [^{11}C]**7** under acid conditions.

The technique[27] of using [^{11}C]methyl triflate to *N*-methylate arylamines within a loop of narrow bore stainless steel tubing is quite general. [^{11}C]**8** was prepared successfully in this manner with a commercially available apparatus (Scheme 4).

NCA [^{11}C]**7** bound specifically to A$_\beta$ plaques in human AD brain slices (Figure 2A). The specific binding was blocked in the presence of excess **3** (Figure 2B), while no binding to normal human brain tissue occurred (Figure 2C, D). These data were encouraging for the further evaluation of carbon-11 labeled **3** as a PET radioligand in vivo.

Dynamic PET scanning in normal mouse, rat, and monkey showed that both [^{11}C]**7** and [^{11}C]**8** gives high brain uptake and quick washout of radioactivity (Figures 3, 4, and 6). Cerebellum typically does not contain a significant amount of A$_\beta$ plaque even in AD.[18] The distribution of radioactivity across normal brain was quite uniform for each radioligand in all three species, as would be expected in the absence of A$_\beta$ plaques. However, the different position of labeling in [^{11}C]**7** and [^{11}C]**8** led to a major difference in the brain radioactivity remaining at 60 min after injection. Correspondingly, the ratios of the radioactivity of maximal uptake to that at 60 min after injection were also quite different, with [^{11}C]**7** being superior in each species. Ratios for [^{11}C]**7** were 18.7, 11.1, and 6.4 in rat, mouse, and monkey, respectively. These ratios are higher than those reported for [^{11}C]**6**, namely, 12.7 and 10.3 for rat and mouse, respectively.[22] A dependence of radioligand pharmacodynamics on position of radiolabel has been observed for some other PET radioligands, a well-known example being [^{11}C]WAY-100635.[33,34] Such differences are invariably attributable to metabolism to different radiometabolites. It was deduced that [^{11}C]**8** produces radiometabolites that enter and persist in brain. Hence, [^{11}C]**8** was not studied further. Further experiments were focused on the stability of [^{11}C]**7** in vitro and in vivo.

[^{11}C]**7** was stable during incubation in vitro with various tissue homogenates, including whole blood and brain of the three species evaluated. However, [^{11}C]**7** was rapidly metabolized in various tissue compartments of living animals. At least three radiometabolites (A−C) were detected in cerebellum, cerebrum, plasma, and urine of rats (Table 2) and also in monkey plasma (Figure 7). Each of these radiometabolites was less lipophilic than **3** according to their faster elution from reverse-phase HPLC (Figures 5 and 7). Radiometabolites A and B were generally predominant in rat brain tissue, plasma, and urine between measurements at 2.33 and 30 min after radioligand injection (Table 2). Ratios of the cerebellar and cerebral parent concentrations to those of the plasma are 55.6 ± 35.8 and 30.5 ± 12.6, respectively. Parent radioligand is the only accumulated or retained species in the brain tissues with its ratio to that in plasma well above 1.0. Similar data obtained from a perfused rat were similar to those of control nonperfused animals, thus confirming the reliability of the observations. Since the radioligand was quite stable in brain homogenates, we deduced that brain radiometabolites originated in the periphery. Therefore, we can conclude that once [^{11}C]**7** enters the brain, it is protected from further extensive metabolism. In the brain and in the presence of target A$_\beta$ amyloid plaques, [^{11}C]**7** should bind to the target with high affinity to deliver a significant signal that should be detectable externally. Furthermore, when carrier **3** was added to the [^{11}C]**7** administered intravenously to rats, a higher proportion of radioactivity in plasma at 10 min was parent radioligand than in the NCA experiment (Table 3). This may indicate that one or more saturable enzymes participated in the metabolism of **3**.

LC−MS analysis of rat brain extract, from the experiment in which CA [^{11}C]**7** was injected into rat, showed a *m*/*z* 270 ion at the same retention time as the *m*/*z* 270 [M + H]$^+$ ion of the *N*-desmethyl compound **2**. Furthermore, the product-ion spectra from MS−MS and MS$^{n(3)}$ analyses of the brain sample were virtually identical to those of **2**. These data identify [^{11}C]**2** as the major radiometabolite of [^{11}C]**7** in rat brain. Metabolism by N-dealkylation has been observed for other IMPY derivatives.[25] The enzyme CYP 3A4, which is highly abundant in gut and liver, is a strong candidate for mediation of these N-dealkylation reactions. The minor radiometabolites, observed in chromatography, were not detected by LC−MS. The similarities between the radiochromatograms of rat (data not shown) and monkey plasma (Figure 7) after administration of NCA [^{11}C]**7** imply the generation of a similar spectrum of radiometabolites and that N-dealkylation is probably the route of metabolism in monkey. This may be the expected route of metabolism in human subjects. Entry of radiometabolites into human brain may prove troublesome to the quantification of specific binding of [^{11}C]**7** to A$_\beta$ plaques. Hence, the further development of this and related ^{11}C-labeled IMPY derivatives may need to address the issue of rapid metabolism.

Conclusions

We identified [^{11}C]**7** as a prospective PET radioligand for imaging A$_\beta$ plaques with PET. This radioligand is simply prepared. It binds selectively and with high affinity to human A$_\beta$ plaques in AD post mortem brain tissue slides. In healthy rats in vivo the radioligand shows a high initial brain uptake of radioactivity and a very fast washout, generating a ratio of the maximal radioactivity to that at 60 min after injection of 18. This ratio predicts a high maximal ratio of radioactivity in vivo between the A$_\beta$ plaque-containing regions and a reference region in AD patients. The analogous ratios in monkeys (7.5−10) well exceed that of [^{11}C]**6** (about 5), an established radioligand for A$_\beta$ plaque imaging. [^{11}C]**7** is slightly unstable in incubations in vitro and is metabolized extensively in vivo, with at least three less lipophilic radiometabolites emerging rapidly in rat and monkey plasma. These radiometabolites are also present in rat brain and urine. Although rapidly generated, these radiometabolites are not retained in brain. Further evaluation of [^{11}C]**7** in human subjects including AD patients is in progress under an FDA-approved exploratory IND. These studies will reveal whether a sizable specific quantifiable PET signal can be obtained with this radioligand or whether further development of related radioligands that avoid problems of metabolism will be necessary.

Experimental Section

Materials. Common reagents were purchased from Aldrich Chemical Co. (Milwaukee, WI), Fluka Chemical Co. (Milwaukee,

WI), Acros (Hampton, NH), or Strem Chemicals (Newburyport, MA) and were used without further purification unless otherwise indicated. DiPPF (1,1′-bis(diisopropylphosphino)ferrocene) was from Strem Chemicals and Pd_2dba_3 [tris(dibenzylideneacetone)dipalladium] from Aldrich. Parent IMPY derivatives were obtained from BioAssay Systems (Hayward, CA). Water was purified through a water purification system comprising a combination of two filters, one Rio, one reservoir, and one Milli-Q synthesis system (Millipore; Bedford, MA). Common solvents were obtained from Fisher Scientific (Pittsburgh, PA). [*N*-methyl-^{3}H]**6** (80 Ci per mmol, radiochemical purity >97%) was obtained from GE Healthcare (Piscataway, NJ). Post mortem brain tissues from an autopsy-confirmed AD case and a healthy control were obtained from the Clinical Brain Disorders Branch, National Institute of Mental Health. Experiments with this material were performed under the regulations of the Ethics Committee of the National Institutes of Health.

Instruments and General Methods. Analytical HPLC was performed using a reverse-phase column (X-bridge C18, 5 μm, 10.0 mm × 250 mm, Waters Corp.; Milford, MA) eluted with concentrated ammonia (0.025%) in acetonitrile−water at 6.2 mL/min. The chromatography system was fitted with a continuous wavelength UV–vis detector (System Gold 168 detector, Beckman; Fullerton, CA) and an autosampler (System Gold 508 autosampler, Beckman). For semipreparative HPLC, a reverse-phase column (Atlantis C18, 5 μm, 30 mm × 150 mm, Waters Corp.) or silica gel column (10 μm, 30 mm × 250 mm, Phenomenex; Torrance, CA) was eluted at 30 mL/min. The HPLC system was fitted with a manual injector (5 mL loop) and a third delivery pump using acetonitrile or ethyl acetate as eluent at 1 mL/min. The purities of compounds were determined with HPLC monitored for absorbance at 254 nm and expressed as area percentage of all peaks.

The ^{1}H and ^{13}C NMR spectra of all compounds were acquired on a DRX 400 instrument (400 MHz for ^{1}H and 100 MHz for ^{13}C, Bruker; Billerica, MA), using the chemical shifts of residual deuterated solvent as the internal standard. Chemical shift (δ) data for the proton and carbon resonances are reported in parts per million (ppm) downfield relative to the internal standard. Mass spectra were acquired using a LCQ^{DECA} LC−MS instrument (Thermo Fisher Scientific; Waltham, MA) fitted with a Luna C18 column (5 μm, 2.0 mm × 150 mm, Phenomenex) eluted at 150 μL/min with a MeOH−H_2O mixture.

High-resolution mass spectra (HRMS) were acquired from the Mass Spectrometry Laboratory, University of Illinois at Urbana−Champaign (Urbana, IL). Either electron spray ionization or electron ionization was used for the ionization. Melting points were measured with a Mel-Temp manual melting point apparatus (Electrothermal, Fisher Scientific) and were uncorrected. A Discover microwave system was used for microwave synthesis (CEM; Matthews, NC).

Methods for the analysis of radioligands and their metabolites in biological samples were generally as previously published.[35] The following are specific details. The initial purity of [^{11}C]**7** to be administered into animals and its stability over 2 h was assessed by HPLC on a Novapak C_{18} column (100 mm × 8 mm, Waters Corp.) housed within a Radial-Pak compression module (RCM-100) with a sentry precolumn and eluted with MeOH/H_2O/Et_3N (70:30:0.1 by volume) at 2.0 mL/min (general method A). Samples were injected onto HPLC through nylon filters (13 mm × 0.45 μm, Iso-Disk, Supelco; Bellefonte, PA). This HPLC system was equipped with an in-line photodiode array absorbance detector (λ = 245 nm, Beckman) and a flow-through Na(Tl) scintillation detector rate meter (Bioscan; Washington, DC). Data from analyses were collected and stored with Bio-Chrome Lite software (Bioscan) and analyzed after decay correction. Recovery of all radioactivity from the HPLC column was checked by an injection of absolute methanol (2 mL) at the end of the chromatography with continued monitoring for radioactivity.

γ-Radioactivity from ^{11}C (>1 μCi) was measured with a calibrated dose calibrator (Atomlab 300, Biodex Medical Systems; Shirley, NY). Low levels of radioactivity (<1 μCi) were measured with a calibrated automatic well-type γ-counter (model 1480 Wizard, Perkin-Elmer; Waltham, MA) having an electronic window set between 360 and 1800 keV (counting efficiency, 51.8%). Decay corrections were performed with a half-life of 20.395 min.[36] ^{3}H was measured with a liquid scintillation counter (Tri-Carb, Perkin-Elmer).

All animal experiments were performed in accordance with the Guide for the Care and Use of Laboratory Animals[37] and were approved by the National Institute of Mental Health Animal Care and Use Committee.

Subsequent numerical data are expressed as the mean ± SD for $n > 2$ or as the mean and range for $n = 2$.

4-(6-(Methylthio)imidazo[1,2-*a*]pyridin-2-yl)aniline (1). 4-(6-Iodo-*H*-imidazo[1,2-*a*]pyridin-2-yl)benzenamine (50 mg, 0.149 mmol), $Pd_2(dba)_3$ (42 mg, 0.0459 mmol), DiPPF (23.5 mg, 0.0562 mmol), $NaSCH_3$ (12.6 mg, 0.180 mmol), and $SnCl(CH_3)_3$ (36 mg, 0.181 mmol) were added to a 10 mL microwave reaction tube. The setup was transferred to a glovebox and anhydrous THF (1.5 mL) added. Reaction was performed in the microwave at 110 °C, 250 psi, and 100 W for 10 min. After the reaction was confirmed to be complete with analytical HPLC, it was quenched with aqueous sodium bicarbonate solution (10% w/v). The mixture was extracted with ethyl acetate (20 mL × 3). The collected organic phase was dried to generate a brown solid, which was further purified through reverse-phase HPLC on a preparative column (250 mm × 30 mm) eluted with a gradient from 5% to 95% acetonitrile over 45 min in a MeCN−H_2O system, giving **1** (9.9 mg, 26%) (t_R = 26 min). Mp 124−127 °C; ^{1}H NMR (400 MHz, $CDCl_3$) δ 8.04 (dd, $^4J_{HH}$ = 1.6 Hz, $^5J_{HH}$ = 0.8 Hz, 1H, Ar−H), 7.71 (m, 2H, Ar−H), 7.65 (s, 1H, Ar−H), 7.51 (d, $^3J_{HH}$ = 9.4 Hz, 1H, Ar−H), 7.13 (dd, $^3J_{HH}$ = 9.4 Hz, $^4J_{HH}$ = 1.8 Hz, 1H, Ar−H), 6.72 (m, 2H, Ar−H), 2.45 (s, 3H, S−CH_3); ^{13}C NMR (400 MHz, $CDCl_3$) δ 146.7, 144.4, 127.6, 127.4 (s, 2C), 124.9, 124.1, 122.2, 117.1, 115.4 (s, 2C), 106.9, 18.7 (s, 1C, S−CH_3); *m*/*z* (ES-MS) 391.3 (15%), 282.3 (13%), 257.1 (7%), 256.1 (100%, (M^+ + H)), 149.0 (18%), 113.1 (10%). HRMS (TOF$^+$): calcd for $C_{14}H_{14}N_3S$ (M^+ + H), 256.0908; found, 256.0912. Error (ppm): 1.6.

***N*-Methyl-4-(6-(methylthio)imidazo[1,2-*a*]pyridin-2-yl)aniline (2).** The procedure was as in the synthesis of **1** except that the iodo compound was 4-(6-iodo-*H*-imidazo[1,2-*a*]pyridin-2-yl)-*N*-methylbenzenamine and gave **2** (20 mg, 50%). Mp 142−144 °C; ^{1}H NMR (400 MHz, CD_3OD) δ 8.24 (dd, $^4J_{HH}$ = 1.8 Hz, $^5J_{HH}$ = 0.9 Hz, 1H, Ar−H), 7.84 (s, 1H, Ar−H), 7.57 (m, 2H, Ar−H), 7.33 (d, $^3J_{HH}$ = 9.4 Hz, 1H, Ar−H), 7.16 (dd, $^3J_{HH}$ = 9.3 Hz, $^4J_{HH}$ = 1.8 Hz, 1H, Ar−H), 6.56 (m, 2H, Ar−H), 2.70 (s, 3H, N-CH_3), 2.40 (s, 3H, S−CH_3); ^{13}C NMR (400 MHz, $CDCl_3$) δ 149.6, 147.0, 144.4, 127.5, 127.3 (s, 2C), 124.9, 122.6, 122.1, 117.1, 112.6 (s, 2C), 106.7, 30.9 (s, 1C, N−CH_3) 18.7 (s, 1C, S−CH_3); *m*/*z* (ES-MS) 271.1 (9%), 270.1 (100%, (M^+ + H)). HRMS (TOF$^+$) calcd for $C_{15}H_{16}N_3S$, 270.1065 (M^+ + H); found, 270.1054. Error (ppm): −4.1.

***N*,*N*-Dimethyl-4-(6-(methylthio)-*H*-imidazo[1,2-*a*]pyridin-2-yl)benzenamine (3).** A 10 mL microwave tube was charged with 4-(6-iodo-*H*-imidazo[1,2-*a*]pyridin-2-yl)-*N*,*N*-dimethylbenzenamine (100 mg, 0.275 mmol), NaSMe (42.4 mg, 0.605 mmol), Me_3SnCl (120 mg, 0.605 mmol), $Pd_2(dba)_3$ (25.2 mg, 0.0275 mmol), DiPPF (11.5 mg, 0.0275 mmol), and THF (4.0 mL) and placed in the microwave at 120 °C, 300 psi, and 250 W for 10 min. The reaction was monitored by analytical HPLC. At the end of the reaction, the reaction mixture was partitioned between K_2CO_3 solution (2 M) and ethyl acetate. The combined organic phase was dried with Na_2SO_4, filtered, and evaporated to leave brown oil. A minimal amount of DMSO was used to dissolve the crude compound, which was then loaded onto a preparative reverse-phase HPLC column. The solvent of the collected peak was removed to afford an oily product. To obtain a crystalline compound, diethyl ether−hexane (1: 5 v/v) was added and the mixture stood at room temperature for about 19 h. The supernatant liquid was removed and the solid washed with excess diethyl ether and hexane and dried overnight to give **3** (40 mg, 51%). Mp 155−164 °C; ^{1}H NMR (400 MHz, CD_3OD) δ 8.34 (s, 1H, Ar−H), 7.96 (s, 1H, Ar−H), 7.73

(d, $^3J_{HH}$ = 9.4 Hz, 2H, Ar−H), 7.44 (d, $^3J_{HH}$ = 9.4 Hz, 1H, Ar−H), 7.26 (dd, $^3J_{HH}$ = 9.4 Hz, $^4J_{HH}$ = 2.2 Hz, 1H, Ar−H), 6.82 (d, $^3J_{HH}$ = 8.9 Hz, 2H, Ar−H), 2.99 (s, 6H, NCH_3), 2.51 (s, 3H, S−CH_3); ^{13}C NMR (400 MHz, CD_3OD) δ 152.3, 147.6, 145.6, 129.0, 128.1, 125.9, 124.6, 122.8, 116.7, 113.9, 108.8, 40.9 (C−S), 17.9 (NCH_3); *m/z* (LC−MS): 286.2 (4%), 285.3 (13%), 284.2 (100%, (M^+ + H)). HRMS (TOF^+) calcd for $C_{16}H_{18}N_3S$ (M^+ + H), 284.1221; found, 284.1215. Error (ppm): −2.4.

Methyl 3-(2-(4-(dimethylamino)phenyl)imidazo[1,2-*a*]pyridin-6-ylthio)propanoate (4). 4-(6-Iodo-*H*-imidazo[1,2-*a*]pyridin-2-yl)-*N*,*N*-dimethylbenzenamine (200 mg, 0.563 mmol), $Pd_2(dba)_3$ (75 mg, 0.0819 mmol), DiPPF (50 mg, 0.120 mmol), methyl 3-mercaptopropanoate (80 μL, 0.738 mmol), and *N*-methyl-*N*-(trimethylstannyl)methanamine (110 μL, 0.674 mmol) were assembled in a microwave tube within a glovebox. Anhydrous THF (1.0 mL) was added and the mixture heated in the microwave oven at 100 °C, 250 psi, and 100 W for 30 min. The reaction was quenched with water, and the mixture was extracted with CH_2Cl_2 (25 mL × 3). The combined organic phases were dried, and the crude residue was further purified by normal phase preparative HPLC eluted with $CHCl_3$ and ethyl acetate, with 0.025% TEA by volume in each solvent, to afford **4** (140 mg, 70%). Mp 116−118 °C; ^{1}H NMR (400 MHz, DMSO-d_6) δ 8.60 (s, 1H, Ar−H), 8.15 (s, 1H, Ar−H), 7.76 (d, $^3J_{HH}$ = 8.4 Hz, 2H, Ar−H), 7.50 (d, $^3J_{HH}$ = 9.3 Hz, 1H, Ar−H), 7.25 (dd, $^3J_{HH}$ = 9.2 Hz, 1H, Ar−H), 6.78 (d, $^3J_{HH}$ = 8.5 Hz, 2H, Ar−H), 3.57 (s, 3H, O−CH_3), 3.10 (t, $^3J_{HH}$ = 6.9 Hz, 2H, SCH_2), 2.94 (s, 6H, NCH_3), 2.62 (t, $^3J_{HH}$ = 6.9 Hz, 2H, CH_2); ^{13}C NMR (400 MHz, CD_3OD) δ 171.6 (−CO_2−), 150.1, 145.8, 143.6, 128.3, 126.5, 121.4, 117.4, 116.2, 112.2, 107.2, 51.5 (OCH_3), 38.9 (NCH_3), 33.7 (CH_2), 29.9 (CH_2); *m/z* (ES-MS): 358.1 (2%), 357.1 (9%), 356.1 (100%, (M^+ + H)). HRMS (TOF^+) calcd for $C_{19}H_{21}N_3O_2S$ (M^+ + H), 356.1433; found, 356.1450. Error (ppm): 4.8.

LogD Measurement. Ligand (3−5 mg) was dissolved in PBS (0.1 M, pH 7.4, 6.0 mL) and *n*-octanol (1.0 mL). The septum-sealed mixture was vortexed for 1 min, shaken vigorously for another 1 min, filtered, held at room temperature for 10 min, and centrifuged at 5000*g* for 10 min. Aliquots of the organic and aqueous layers were sampled through the septum by syringe. An aliquot of octanol layer (5.0 μL) was added to acetonitrile (5.0 mL) to prepare a stock solution. Both aqueous and organic phases (1.0 mL each) were analyzed for ligand by HPLC (X-bridge C18, 5 μm, 10.0 mm × 250 mm, Waters Corp.) eluted at 2.0 mL/min with MeCN/water containing concentrated ammonia (0.025% by volume) in each component, using a gradient from 5% to 95% MeCN over 15 min. Partition coefficients (*P*) were calculated as the ratio of ligand concentrations between the organic and aqueous phases.

In Vitro Binding Assay. Human AD brain tissue was homogenized in phosphate-buffered saline (PBS) at 1:500 dilution in volume, and aliquots of this suspension (100 μL) were added to each of four tubes (total 48 in a rack). A solution of [^{3}H]**6** (2.7 × 10^{-4} μCi/μL) in PBS (100 μL) was added to each tube. Nonradioactive **6** or other displacer was dissolved in DMSO to give a 1 mM stock solution, which was further diluted with DMSO to give solutions ranging from 1 × 10^{-5} to 10^{-10} M; 10 μL of solution was added to each tube. After assembly of the components listed above in each tube (made up to a total volume of 1.0 mL by PBS), the tubes were vortexed and then incubated for 2 h at 37 °C. After separation of tube contents with a cell harvester, the filter paper (GF/B, Whatman, pretreated with 0.5% polyethyleneimine solution) was washed with PBS (3 mL × 3). The filters were placed in 7 mL plastic vials, and scintillation fluid (4 mL) was added to each. After overnight incubation, the scintillation vials were counted for radioactivity. The collected data were analyzed using GraphPad Prism 4, version 4.03 (GraphPad Software; San Diego, CA), with "one site competition" curve-fitting. K_i values were calculated according to the Cheng−Prusoff equation:[38]

$$K_i = \frac{IC_{50}}{1 + \frac{[L]}{K_D}}$$

where [L] is the concentration (0.4 nM) and K_D the equilibrium constant of the reference radioligand ([^{3}H]**6**). The latter was determined with "Scatchard analysis of homologous displacement" from multiple runs with self-displacement from AD brain tissue.

Production of Labeling Agents. NCA [^{11}C]carbon dioxide was produced by irradiation of nitrogen (∼225 psi) containing a low concentration of oxygen (1%) for 40 min with a proton beam (16 MeV, 40 μA) produced from a PETtrace cyclotron (GE Medical Systems; Milwaukee, WI). The irradiation produced about 1.4 Ci of [^{11}C]carbon dioxide. [^{11}C]Carbon dioxide was converted into [^{11}C]iodomethane by reduction to [^{11}C]methane and then high temperature iodination within a Microlab module (GE MS PET Systems AB, GE Healthcare; Piscataway, NJ). [^{11}C]Methyl triflate was produced by passing [^{11}C]iodomethane in helium (30 mL/min) over heated (190 °C) silver triflate.[39]

Preparation of [^{11}C]7. Methyl 3-(2-(4-(dimethylamino)phenyl)imidazo[1,2-*a*]pyridin-6-ylthio)propanoate (**4**, 0.5 mg, 1.4 μmol) in acetonitrile (0.40 mL) and *tert*-butylimino-tris(dimethylamino-)phosphorane (7 μL of 0.5 M stock solution in MeCN, 3.5 μmol) were loaded into a septum-sealed reaction vial (1 mL neck vial, Waters Corp.) of a Synthia apparatus (Uppsala University PET Center, GE Healthcare; Uppsala, Sweden). [^{11}C]Iodomethane was then swept into the vial from the MicroLab module in a stream of helium at 15 mL/min. After reaction was allowed to proceed at 80 °C for 5 min, [^{11}C]**7** was separated by HPLC on a Luna C18 column (10 μm, 4.6 mm × 250 mm, Phenomenex) eluted at 6 mL/min with MeCN/0.1% H_3PO_4 (20:80 v/v) changed linearly to 50:50 (v/v) over 20 min. Eluate was monitored for absorbance at 350 nm and radioactivity. The fraction containing [^{11}C]**7** (t_R = 9.3 min) was collected and neutralized with aqueous $NaHCO_3$ solution (8.4% w/v) and then rotary-evaporated to dryness (80 °C water bath). The residue of [^{11}C]**7** was formulated in sterile saline for injection USP (0.9% w/v, 10 mL) plus ethanol USP (0.9 mL) containing polysorbate 80 (20 mg) and then sterile-filtered into a sterile and pyrogen-free dose vial.

This product was analyzed by HPLC on a Luna C18 column (10 μm, 4.6 mm × 250 mm, Phenomenex) eluted with 0.1% phosphoric acid (84% w/w) in water (pH ∼ 2.35) (A)/acetonitrile (B) at 2 mL/min with mobile phase composition run at 70% A for 2 min and then decreased to 40% A over 15 min. Eluate was monitored for absorbance at 350 nm and for radioactivity. Retention times were as follows: 5.2 min for **4**, 7.2 min for [^{11}C]**7**, and 11 min for [^{11}C]iodomethane. The response of the analytical system was calibrated for mass of **3** to allow specific radioactivity to be calculated.

Preparation of [^{11}C]8. The labeling reaction between precursor **2** and [^{11}C]methyl triflate was performed in a commercial loop system (Bioscan).[27] The helium flow through the apparatus was adjusted to 30 mL/min. Precursor **2** (0.5 mg, 1.9 μmol) was dissolved in methyl ethyl ketone (80 μL) and loaded into the loop at about 1 min before the end of radionuclide production. [^{11}C]Methyl triflate was passed into the loop in helium at 30 mL/min, and the reaction was allowed to proceed for 2 min at room temperature. The reaction mixture was injected onto a C-18 Luna column (10 μm, 4.6 × 250 mm, Phenomenex) eluted with MeCN/50 mM $HCOONH_4$ (60:40 v/v, pH 7.2) at 6 mL/min. Eluate was monitored for absorbance at 350 nm and radioactivity. The fraction containing [^{11}C]**8** (t_R = 7.5 min) was well separated from [^{11}C]iodomethane (t_R ≈ 3−4 min), **2** (t_R ≈ 5.3 min) and other products and was collected and then rotary-evaporated to dryness (80 °C water bath). The residue was formulated in sterile saline (10 mL) containing ethanol (5% v/v). This product was analyzed by radio-HPLC as described for [^{11}C]**7**.

Autoradiography of [^{11}C]7 to Post Mortem Human Brain Tissue. Coronal sections of cerebrum from a confirmed case of AD (female, 59 year old, post mortem interval (PMI) of 47.5 h) and a normal control (female, 64 year old, PMI of 28.5 h) were frozen rapidly in an equal mixture of dry ice and isopentane, sealed in a plastic bag, and stored at −76 °C before sectioning. Frozen blocks of the medial temporal lobe (hippocampal region) were sectioned at a thickness of 14 μm, mounted on gelatin-coated glass

slides, dried, and stored under desiccant at −76 °C. Before use, slide-mounted tissue sections were removed from the freezer, thawed at room temperature for 20 min, and air-dried.

Ligand **3** (1.0 mg) was dissolved in DMSO (3.529 mL), resulting in a stock solution of 1 mM, which was then further diluted with DMSO to 0.1 mM and then diluted with PBS to 1 μM. The AD tissue and normal tissue slides were pretreated with either a stock solution of **3** or PBS for 20 min at room temperature. All slides were incubated for 20 min at room temperature in [^{11}C]**7** formulation solution (0.3 mCi). They were then dipped in ethanol for 5 min. The slides were dried on a hot plate with a stream of cold air and placed in a cassette with the exposed sides facing up. The phosphor imaging plate was held with the blue side down. The entire cassette was placed in the dark at room temperature overnight for ^{11}C-labeling. Digital autoradiography was acquired using a FUJI BAS 5000 phosphorimager (FUJI, Tokyo, Japan) with a resolution of 25 μm.

Stability of NCA [^{11}C]7 in Rat and Monkey Whole Blood in Vitro. Whole blood (1 mL) from monkey or rat was placed in a polypropylene test tube (13 mm × 60 mm) with 25.0 μCi (30 μL) or 46.5 μCi (15 μL) of NCA [^{11}C]**7**, respectively. The samples were then incubated at 37 °C in a reciprocating shaker water bath (model 25, Fisher Scientific; Pittsburgh, PA) at 60 oscillations per minute. The radioactive whole blood was sampled (50−100 μL) at 60 and 90 min and then placed in MeCN (300 μL) that had been spiked with **3**. The mixture was mixed well. Then water (1.0 mL) was added and the solution mixed well again. All the MeCN samples were counted in a γ-counter and then centrifuged at 10000*g* for 1 min. The supernatant liquids were analyzed with HPLC general method A. The precipitates were measured for radioactivity in a γ-counter to allow calculation of the recovery of radioactivity into acetonitrile.

Stability of NCA [^{11}C]7 in Rat Brain in Vitro. One healthy rat (350 g) was anesthetized with 1.5% isoflurane and 98.5% O_2. Blood (about 10 mL) was drawn by cardiac puncture and used in the above-described whole blood stability experiment. The rat was then perfused with saline (0.9% w/v, 12 mL) through the exposed heart right atrium while the aorta was severed. The excised brain (1.75 g) was homogenized with saline (3 mL) while cooled on ice with a Tissue-Tearor (model 985-370, Biospec Products Inc.; Bartlesville, OK). Formulated [^{11}C]**7** (186 μCi) was added to the brain homogenate and then incubated in a reciprocating shaker at 37 °C. For HPLC analyses, aliquots (100 μL) from this mixture were removed at 90 min and placed in acetonitrile (300 μL) that had been spiked with **3**. The mixture was mixed well, and then water (100 μL) was added and the solution mixed well again. All the acetonitrile samples were counted in a γ-counter and then centrifuged at 10000*g* for 1 min. The supernatant liquids were analyzed with HPLC general method A. The precipitates were then counted in a γ-counter for calculating the recovery of radioactivity into the acetonitrile.

Evaluation of Radioligands in Normal Rodents in Vivo with PET. For radioligand injection, a 30 gauge needle was attached to a polyethylene catheter (PE 10) and inserted into the tail vein of a mouse or the penis vein of a male rat. The needle and catheter were secured with tissue adhesive and tape. For dynamic scanning, heads and bodies of mice and rats were fixed with tape and kept under 1.5% isoflurane anesthesia via a nose cone. Body temperature was monitored with a rectal probe and maintained between 36 and 37 °C. Then formulated NCA radioligand (400−450 μCi, volume of 0.1−0.2 mL) was injected and flushed with heparinized saline (0.070 mL).

For PET imaging, we used the NIH Advanced Technology Laboratory Animal Scanner (ATLAS) with an effective transaxial field of view of 6.0 cm and an axial field of view of 2.0 cm.[40] Dynamic scanning began at the time of injection and lasted for 90 min. Data were reconstructed into 17 coronal slices with a voxel size of 0.56 mm × 0.56 mm × 1.12 mm. No attenuation or scatter corrections were applied. The dual-layered phoswich detector design of the scanner and 3D OSEM (ordered subset expectation maximization) reconstruction achieved a resolution of 1.6 mm at the center of the field of view. Tomographic images were analyzed with PMOD 2.6 (pixelwise modeling computer software, PMOD Group; Zurich, Switzerland).[41] Two regions of interest, cerebrum and cerebellum, were delineated, and time−activity curves were calculated.

Emergence of Radiometabolites of NCA [^{11}C]7 in Normal Rat. Various minutes (2.33, 2.83, and 30 min) after the penile venous injection of NCA [^{11}C]**7** (0.82−3.6 mCi, SR 0.9−1.9 Ci/μmol) into each of eight rats, a large blood sample (about 5−10 mL) was drawn from each and placed on ice until analysis. Urine was aspirated from the urinary bladder and analyzed within a few minutes with HPLC by general method A. The rat was then immediately sacrificed by decapitation, and the cerebrum and cerebellum were excised and placed on ice until analysis. One rat was perfused with heparinized saline (0.9% w/v, 12 mL) through the heart after severing the right aortic vessel. The perfusion was continued until the perfusate ran clear of blood. The brain tissues were placed in acetonitrile (1.5 mL) and measured for radioactivity in the γ-counter. The tissues were then homogenized along with nonradioactive **3** (50 μg). After the addition of water (500 μL), the tissues were further homogenized and measured in the γ-counter. The homogenates were centrifuged at 10000*g* for 1 min. The supernatant liquids were then analyzed with HPLC (general method A). After separation of the plasma from blood cells, plasma samples (50 μL) were counted in the γ-counter and aliquots (450 μL) placed in acetonitrile (700 μL) along with carrier **3** (5 μg). After the samples were mixed well, water (100 μL) was added and the samples were further mixed well and measured in a γ-counter. The samples were then centrifuged and the clear supernatant liquids analyzed by radio-HPLC (general method A). All precipitates were measured in the γ-counter so that recoveries of radioactivity into the supernatants could be calculated.

The % SUV due to parent radioligand or radiometabolite only was calculated by multiplying the total % SUV by the fraction obtained by HPLC using the following equation:

$$\%\ \mathrm{SUV} = \left(\frac{\text{tissue activity/tissue (g)}}{\text{injected activity}} \times 100 \times \text{body weight (g)}\right) \times \text{HPLC fraction}$$

Emergence of Rat Brain Metabolites of CA [^{11}C]7 in Rat. One healthy rat (311 g) was anesthetized with 1.5% isoflurane in O_2. The rat body temperature was maintained around 37 °C with a heating pad. To ensure the expression of urine, the rat was infused with saline (0.9% w/v, 5.0 mL) for 30 min. The rat was then injected with CA [^{11}C]**7** (950 μCi, 7.14 μmol carrier, 22.9 μmol carrier per kg, specific radioactivity 0.113 mCi/μmol) formulated in saline (0.9% w/v, 2.0 mL) containing ethanol (10% v/v) and Tween-80 (5% v/v). Briefly, the dose was prepared as follows: **3** (2.02 mg, 7.135 nmol) was dissolved in ethanol (200 μL) and then Tween-80 (100 μL) added. The mixture was vortexed. To the resulting solution, saline (0.9% w/v) was added in increments of 200 μL with vortexing on each addition until the total volume became 2.0 mL. Radioactivity was added to the vial that contained the nonradioactive **3**, mixed well, and measured in a dose calibrator. The now low specific activity dose was then drawn, the vial measured again, and the dose injected into the rat. The dose was infused through the penile vein over 5.0 min. After 10 min, the urinary bladder of the rat was exposed and urine (∼850 μL) withdrawn into a syringe. The brain (1.6 g) and cerebellum (0.31 g) were excised, and each was placed in MeCN (1.5 mL) along with carrier **3** (∼100 μg). The tissues were then homogenized with the "Tissue-Tearor". Water (500 μL) was added and the mixture rehomogenized. The homogenates were centrifuged at 10000*g* for 1.0 min. The clear supernatant liquids were decanted and placed in fresh polypropylene tubes. The precipitates were rehomogenized with acetonitrile (1.5 mL) followed by water (500 μL) and centrifuged as before. The second supernatants were combined with the previous ones. The tissue radioactivities were further separated from the parent by HPLC and the radiometabolite fractions I and II collected for storage at −70 °C until LC−MS analysis. Aliquots (1 mL) from rat brain extracts were concentrated with a SpeedVac evaporator

(Thermo Fisher Scientific) and the residues reconstituted in mobile phase A (H_2O/MeOH/AcOH, 90:10:0.5 by volume, 200 μL). The samples were centrifuged (10000*g*, 1 min) and the supernatant liquids transferred to an autosampler vial for injection into LC−MS. Because only a small amount of radioactivity was excreted, the urine was diluted 2.5-fold with acetonitrile and injected onto the HPLC. A very small volume was saved for LC−MS analysis.

A reverse-phase HPLC column (Synergi Fusion-RP, 4 μm, 150 mm × 2 mm, Phenomenex) was used for the separation of the metabolites of CA [^{11}C]**7**. A gradient analysis was performed with mobile phase A (listed above) and mobile phase B composed of methanol with 0.5% acetic acid. Initially, the column was equilibrated with mobile phase 80% A and 20% B at 150 μL/min. The sample (5 μL) was injected, and after 1 min the pump ran a linear gradient reaching 20% A and 80% B over 10 min and then was held isocratic at this composition for 3 min. At the end of the run, the mobile phase was returned to the initial composition and equilibrated with elution for 3 min at 250 μL/min.

The separated components from the brain extract were ionized by electrospray with the following settings: sheath gas flow 64 units, auxiliary gas flow 10 units, capillary temperature 260 °C, capillary voltage 26 V, and spray voltage 5 kV. For MS analysis, ions ranging between *m*/*z* 150 and 600 were acquired. MS−MS and $MS^{n(3)}$ analyses of **3** and its metabolites were performed with an isolation width of 1.5 amu and a collision energy level at 44%.

Reference solutions (2 ng/μL) of **3** and **2** were prepared in mobile phase A and injected (1−2 μL) into LC−MS and analyzed in a similar manner to brain samples.

Evaluation of Radioligands in Monkey in Vivo with PET. A male rhesus monkey (15 kg) was initially immobilized with ketamine (15 mg/kg) and subsequently anesthetized with isoflurane (1.5%) for the duration of the experiment. The monkey was placed prone in the PET camera (HRRT, Siemens/CPS; Knoxville, TN). A fixation device was used to secure the monkey's head during scanning. A urinary catheter was inserted and clamped so that the activity overlaying the bladder represented the total urinary excretion during the scan. Electrocardiogram, body temperature, and heart and respiration rates were measured throughout the experiment. Body temperature was controlled and monitored by a forced-air temperature management unit (Bair Hugger model 505, Arizant Healthcare Inc.; MN). The scanner consisted of eight flat panel detectors with a transaxial and axial coverage of 31.2 and 25.2 cm, respectively. The scanner is also equipped with dual-layered phoswich detector allowing depth of interaction. Dynamic PET scans were acquired in 64-bit list mode format, following the intravenous administration of [^{11}C]**7** or [^{11}C]**8** (2.9 mCi). The scan lasted for 2 h containing 33 frames with duration ranging from 30 s to 5 min. Data were reconstructed into a 256 × 256 × 207 image matrix (voxel size 1.21 × 1.21 × 1.23 mm), using a 3D list mode OSEM algorithm.[42] The reconstructed image resolution was 2.5 mm. Transmission scan was acquired with a rotating ^{137}Cs point source for 6 min and used to correct for attenuation. A model-based scatter correction was applied. Tomographic images were analyzed with PMOD 2.6.[41] Time−activity curves were calculated in % SUV for volume of interest (VOIs), defined by coregistration with MRI (see below) and compared for uptake and washout between different brain regions.

Coregistration of PET Data with MRI. All frames of the original reconstructed PET data were summed and then coregistered to a T_1-weighted magnetic resonance (MR) image acquired separately on a 1.5 T Signa MR scanner (GE Medical Systems) with image analysis software MEDx (Sensor Systems Inc.; Sterling, VA). The summed PET image was fused with the coregistered MR image with an image fusion tool in PMOD. Several VOIs for the source organs were then manually defined on this fused image with anatomical structures identified on the MR image.

Emergence of Radiometabolites of NCA [^{11}C]7 in Monkey Plasma. A monkey (14.9 kg) was anesthetized with 1.6% isoflurane in oxygen and as a baseline experiment (test) was administered [^{11}C]**7** (2.31 mCi, 1.35 Ci/μmol, 1.71 nmol carrier, 0.11 nmol carrier per kg, pH ∼ 8−9) formulated in 5% ethanolic saline adjusted to basic pH with sodium bicarbonate. A second baseline (retest) experiment was performed in the same monkey injected with [^{11}C]**7** (3.99 mCi, 1.93 Ci/μmol, 2.07 nmol carrier, 0.14 nmol carrier per kg, pH 4.5−5.0). Heparinized venous blood samples (2.0 mL) from both experiments were drawn at 10 and 30 min after injection. Blood samples were centrifuged at 1800*g* for 1.5 min. Plasma samples (450 μL) were then placed in MeCN (700 μL) and spiked with **3**. The MeCN−plasma mixture was measured for total radioactivity in a γ-counter and then centrifuged at 10000*g* for 1 min and analyzed by radio-HPLC (general method A). The activities remaining in the precipitates were used to calculate the percent recovery of activity into the acetonitrile analytes. The % SUV values for each component detected by radio-HPLC were calculated as described above for the rat experiment.

Acknowledgment. This research was supported by the Intramural Research Program of the National Institutes of Health, specifically the National Institute of Mental Health. We gratefully thank Dr. Shuiyu Lu (MIB, NIMH), Kun Park (MIB, NIMH), and Edward Tuan (MIB, NIMH) for experimental assistance and Dr. Joel E. Kleinman (CDBD, NIMH) for post mortem human brain tissues and useful discussions. We also thank the NIH PET Department for carbon-11 production and successful completion of the scanning experiments, PMOD Technologies for providing the image analysis software, and the NIMH Psychoactive Drug Screening Program (PDSP) for performing assays. The PDSP is directed by Bryan L. Roth, Ph.D., with project officer Jamie Driscoll (NIMH) at the University of North Carolina Chapel Hill (Contract No. NO1MH32004).

Supporting Information Available: Purity data and HPLC chromatograms of compounds **1**−**4**. This material is available free of charge via the Internet at http://pubs.acs.org.

References

(1) Selkoe, D. J. Alzheimer's disease: genes, proteins, and therapy. *Physiol. Rev.* **2001**, *81*, 741–766.
(2) Selkoe, D. J. Alzheimer disease: mechanistic understanding predicts novel therapies. *Ann. Intern. Med.* **2004**, *140*, 627–638.
(3) Hardy, J.; Selkoe, D. J. The amyloid hypothesis of Alzheimer's disease: progress and problems on the road to therapeutics. *Science* **2002**, *297*, 353–356.
(4) Cummings, J. L. Alzheimer's disease. *N. Engl. J. Med.* **2004**, *351*, 56–67.
(5) Mattson, M. P. Pathways towards and away from Alzheimer's disease. *Nature* **2004**, *430*, 631–639.
(6) Wilquet, V.; De Strooper, B. Amyloid-beta precursor protein processing in neurodegeneration. *Curr. Opin. Neurobiol.* **2004**, *14*, 582–588.
(7) Rogaeva, E.; Meng, Y.; Lee, J. H.; Gu, Y.; Kawarai, T.; Zou, F.; Katayama, T.; Baldwin, C. T.; Cheng, R.; Hasegawa, H.; Chen, F.; Shibata, N.; Lunetta, K. L.; Pardossi-Piquard, R.; Bohm, C.; Wakutani, Y.; Cupples, L. A.; Cuenco, K. T.; Green, R. C.; Pinessi, L.; Rainero, I.; Sorbi, S.; Bruni, A.; Duara, R.; Friedland, R. P.; Inzelberg, R.; Hampe, W.; Bujo, H.; Song, Y. Q.; Andersen, O. M.; Willnow, T. E.; Graff-Radford, N.; Petersen, R. C.; Dickson, D.; Der, S. D.; Fraser, P. E.; Schmitt-Ulms, G.; Younkin, S.; Mayeux, R.; Farrer, L. A.; George-Hyslop, P. The neuronal sortilin-related receptor SORL1 is genetically associated with Alzheimer disease. *Nat. Genet.* **2007**, *39*, 168–177.
(8) Farrer, L. A.; Cupples, L. A.; Haines, J. L.; Hyman, B.; Kukull, W. A.; Mayeux, R.; Myers, R. H.; Pericak-Vance, M. A.; Risch, N.; van Duijn, C. M. Effects of age, sex, and ethnicity on the association between apolipoprotein E genotype and Alzheimer disease. A meta-analysis. APOE and Alzheimer Disease Meta Analysis Consortium. *JAMA, J. Am. Med. Assoc.* **1997**, *278*, 1349–1356.
(9) Saunders, A. M.; Strittmatter, W. J.; Schmechel, D.; George-Hyslop, P. H.; Pericak-Vance, M. A.; Joo, S. H.; Rosi, B. L.; Gusella, J. F.; Crapper-MacLachlan, D. R.; Alberts, M. J. Association of apolipoprotein E allele epsilon 4 with late-onset familial and sporadic Alzheimer's disease. *Neurology* **1993**, *43*, 1467–1472.
(10) Bertram, L.; Hsiao, M.; McQueen, M. B.; Parkinson, M.; Mullin, K.; Blacker, D.; Tanzi, R. E. The LDLR locus in Alzheimer's disease: a family-based study and meta-analysis of case-control data. *Neurobiol. Aging* **2007**, *28*, 18–21.

(11) Bertram, L.; McQueen, M. B.; Mullin, K.; Blacker, D.; Tanzi, R. E. Systematic meta-analyses of Alzheimer disease genetic association studies: the AlzGene database. *Nat. Genet.* **2007**, *39*, 17–23.
(12) Braak, H.; Braak, E. Neuropathological stageing of Alzheimer-related changes. *Acta Neuropathol.* **1991**, *82*, 239–259.
(13) Tanzi, R. E. Molecular genetics of Alzheimer's disease and the amyloid beta peptide precursor gene. *Ann. Med.* **1989**, *21*, 91–94.
(14) Engler, H.; Forsberg, A.; Almkvist, O.; Blomquist, G.; Larsson, E.; Savitcheva, I.; Wall, A.; Ringheim, A.; Långström, B.; Nordberg, A. Two-year follow-up of amyloid deposition in patients with Alzheimer's disease. *Brain* **2006**, *129*, 2856–2866.
(15) Small, G. W.; Kepe, V.; Ercoli, L. M.; Siddarth, P.; Bookheimer, S. Y.; Miller, K. J.; Lavretsky, H.; Burggren, A. C.; Cole, G. M.; Vinters, H. V.; Thompson, P. M.; Huang, S. C.; Satyamurthy, N.; Phelps, M. E.; Barrio, J. R. PET of brain amyloid and tau in mild cognitive impairment. *N. Engl. J. Med.* **2006**, *355*, 2652–2663.
(16) Newberg, A. B.; Wintering, N. A.; Plossl, K.; Hochold, J.; Stabin, M. G.; Watson, M.; Skovronsky, D.; Clark, C. M.; Kung, M. P.; Kung, H. F. Safety, biodistribution, and dosimetry of ^{123}I-IMPY: a novel amyloid plaque-imaging agent for the diagnosis of Alzheimer's disease. *J. Nucl. Med.* **2006**, *47*, 748–754.
(17) Cai, L.; Innis, R. B.; Pike, V. W. Radioligand development for PET imaging of β-amyloid-current status. *Curr. Med. Chem.* **2007**, *14*, 19–52.
(18) Klunk, W. E.; Engler, H.; Nordberg, A.; Wang, Y.; Blomqvist, G.; Holt, D. P.; Bergstrom, M.; Savitcheva, I.; Huang, G. F.; Estrada, S.; Ausen, B.; Debnath, M. L.; Barletta, J.; Price, J. C.; Sandell, J.; Lopresti, B. J.; Wall, A.; Koivisto, P.; Antoni, G.; Mathis, C. A.; Långström, B. Imaging brain amyloid in Alzheimer's disease with Pittsburgh Compound-B. *Ann. Neurol.* **2004**, *55*, 306–319.
(19) Price, J. C.; Klunk, W. E.; Lopresti, B. J.; Lu, X.; Hoge, J. A.; Ziolko, S. K.; Holt, D. P.; Meltzer, C. C.; DeKosky, S. T.; Mathis, C. A. Kinetic modeling of amyloid binding in humans using PET imaging and Pittsburgh Compound-B. *J. Cereb. Blood Flow Metab.* **2005**, *25*, 1528–1547.
(20) Naslund, J.; Schierhorn, A.; Hellman, U.; Lannfelt, L.; Roses, A. D.; Tjernberg, L. O.; Silberring, J.; Gandy, S. E.; Winblad, B.; Greengard, P. Relative abundance of Alzheimer Aβ amyloid peptide variants in Alzheimer disease and normal aging. *Proc. Natl. Acad. Sci. U.S.A.* **1994**, *91*, 8378–8382.
(21) Laruelle, M.; Slifstein, M.; Huang, Y. Relationships between radiotracer properties and image quality in molecular imaging of the brain with positron emission tomography. *Mol. Imaging Biol.* **2003**, *5*, 363–375.
(22) Mathis, C. A.; Wang, Y.; Holt, D. P.; Huang, G. F.; Debnath, M. L.; Klunk, W. E. Synthesis and evaluation of ^{11}C-labeled 6-substituted 2-arylbenzothiazoles as amyloid imaging agents. *J. Med. Chem.* **2003**, *46*, 2740–2754.
(23) Zhuang, Z. P.; Kung, M. P.; Wilson, A.; Lee, C. W.; Plossl, K.; Hou, C.; Holtzman, D. M.; Kung, H. F. Structure−activity relationship of imidazo[1,2-*a*]pyridines as ligands for detecting β-amyloid plaques in the brain. *J. Med. Chem.* **2003**, *46*, 237–243.
(24) Cai, L.; Cuevas, J.; Temme, S.; Herman, M. M.; Dagostin, C.; Widdowson, D. A.; Innis, R. B.; Pike, V. W. Synthesis and structure−affinity relationships of new 4-(6-iodo-*H*-imidazo[1,2-*a*]pyridin-2-yl)-*N*,*N*-dimethylbenzeneamine derivatives as ligands for human betaamyloid plaques. *J. Med. Chem.* **2007**, *50*, 4746–4758.
(25) Cai, L.; Chin, F. T.; Pike, V. W.; Toyama, H.; Liow, J. S.; Zoghbi, S. S.; Modell, K.; Briard, E.; Shetty, H. U.; Sinclair, K.; Donohue, S.; Tipre, D.; Kung, M. P.; Dagostin, C.; Widdowson, D. A.; Green, M.; Gao, W.; Herman, M. M.; Ichise, M.; Innis, R. B. Synthesis and evaluation of two ^{18}F-labeled 6-iodo-2-(4′-*N*,*N*-dimethylamino)phenylimidazo[1,2-*a*]pyridine derivatives as prospective radioligands for β-amyloid in Alzheimer's disease. *J. Med. Chem.* **2004**, *47*, 2208–2218.
(26) Cai, L.; Cuevas, J.; Peng, Y. Y.; Pike, V. W. Rapid palladium-catalyzed cross-coupling in the synthesis of aryl thioethers under microwave conditions. *Tetrahedron Lett.* **2006**, *47*, 4449–4452.
(27) Wilson, A. A.; Garcia, A.; Chestakova, A.; Kung, H.; Houle, S. A rapid one-step radiosynthesis of the β-amyloid imaging radiotracer *N*-methyl-[^{11}C]-2-(4′-methylaminophenyl)-6-hydroxybenzothiazole([^{11}C]-6-OH-BTA-1). *J. Labelled Compd. Radiopharm.* **2004**, *47*, 679–682.
(28) Klunk, W. E.; Lopresti, B. J.; Debnath, M. L.; Holt, D. P.; Wang, Y.; Huang, G.-F.; Shao, L.; Lefterov, I.; Koldamova, R.; Ikonomovic, M.; DeKosky, S. T.; Mathis, C. A. Amyloid deposits in transgenic PS1/APP mice do not bind the amyloid PET tracer, PIB, in the same manner as human brain amyloid. *Neurobiol. Aging* **2004**, *25*, 232–233.
(29) Pike, V. W. Positron-emitting radioligands for studies in vivo. Probes for human psychopharmacology. *J. Psychopharmacol.* **1993**, *7*, 139–158.
(30) Waterhouse, R. N. Determination of lipophilicity and its use as a predictor of blood−brain barrier penetration of molecular imaging agents. *Mol. Imaging Biol.* **2003**, *5*, 376–389.
(31) Schou, M.; Pike, V. W.; Varrone, A.; Gulyas, B.; Farde, L.; Halldin, C. Synthesis and PET evaluation of (*R*)-[*S*-methyl-^{11}C]thionisoxetine, a candidate radioligand for imaging brain norepinephrine transporters. *J. Labelled Compd. Radiopharm.* **2006**, *49*, 1007–1019.
(32) Becht, J. M.; Wagner, A.; Mioskowski, C. Facile introduction of SH group on aromatic substrates via electrophilic substitution reactions. *J. Org. Chem.* **2003**, *68*, 5758–5761.
(33) Pike, V. W.; McCarron, J. A.; Lammerstma, A. A.; Hume, S. P.; Poole, K.; Grasby, P. M.; Malizia, A.; Cliffe, I. A.; Fletcher, A.; Bench, C. J. First delineation of 5-HT$_{1A}$ receptors in human brain with PET and [^{11}C]WAY-100635. *Eur. J. Pharmacol.* **1995**, *283*, R1–R3.
(34) Hume, S. P.; Ashworth, S.; Opacka-Juffry, J.; Ahier, R. G.; Lammertsma, A. A.; Pike, V. W.; Cliffe, I. A.; Fletcher, A.; White, A. C. Evaluation of [*O*-methyl-^{3}H]WAY-100635 as an in vivo radioligand for 5-HT$_{1A}$ receptors in rat brain. *Eur. J. Pharmacol.* **1994**, *271*, 515–523.
(35) Zoghbi, S. S.; Shetty, H. U.; Ichise, M.; Fujita, M.; Imaizumi, M.; Liow, J. S.; Shah, J.; Musachio, J. L.; Pike, V. W.; Innis, R. B. PET imaging of the dopamine transporter with ^{18}F-FECNT: a polar radiometabolite confounds brain radioligand measurements. *J. Nucl. Med.* **2006**, *47*, 520–527.
(36) Weber, D. A.; Eckerman, K. F.; Dillman, L. T.; Ryman, J. C. *MIRD: Radionuclide Data and Decay Schemes*; Society of Nuclear Medicine: New York, 1989.
(37) Clark, J. D.; Baldwin, R. L.; Bayne, K. A.; Brown, M. J.; Gebhart, G. F.; Gonder, J. C.; Gwathmey, J. K.; Keeling, M. E.; Kohn, D. F.; Robb, J. W.; Smith, O. A.; Steggerda, J.-A. D.; VandeBerg, J. L. *Guide for the Care and Use of Laboratory Animals*; National Academy Press: Washington, DC, 1996.
(38) Cheng, Y.; Prusoff, W. H. Relationship between inhibition constant (K_I) and concentration of inhibitor which causes 50% inhibition (IC_{50}) of an enzymatic-reaction. *Biochem. Pharmacol.* **1973**, *22*, 3099–3108.
(39) Jewett, D. M. A simple synthesis of [C-11] methyl triflate. *Appl. Radiat. Isot.* **1992**, *43*, 1383–1385.
(40) Green, M. V.; Seidel, J.; Vaquero, J. J.; Jagoda, E.; Lee, I.; Eckelman, W. C. High resolution PET, SPECT and projection imaging in small animals. *Comput. Med. Imaging Graphics* **2001**, *25*, 79–86.
(41) Mikolajczyk, K.; Szabatin, M.; Rudnicki, P.; Grodzki, M.; Burger, C. A JAVA environment for medical image data analysis: initial application for brain PET quantitation. *Med. Informatics (London)* **1998**, *23*, 207–214.
(42) Carson, R. E.; Barker, W. C.; Liow, J.-S.; Yao, R.; Thada, S.; Zhao, Y.; Iano-Fletcher, A.; Lenox, M. List-mode reconstruction for the HRRT. *J. Nucl. Med.* **2004**, (Suppl. 45), 105P.

JM700970S